Supplementary information for
Grain alignment in hexaferrite permanent magnets by compaction at room and elevated temperature

By Jacob L. Valentin, Frederik H. Gjørup, Cecilie G. Knudsen & Mogens Christensen

Powder X-ray diffraction of precursor powders

Powder X-ray diffraction (PXRD) was performed on the precursor powders to confirm phase and obtain a size estimate, extracted parameters from the refinements performed in Fullprof[1] can be found in Table S1.

Table S1: Summary of PXRD refinement results on precursor powders MRT, M600 & M1000

	MRT	M600	M1000
Reliability factors (all points, not background corrected)			
R_p (%)	7.10	4.90	4.41
R_{wp} (%)	8.91	6.37	5.71
R_{exp} (%)	3.83	4.51	4.35
χ^2	5.72	1.99	1.72
Reliability factors (all points, background corrected)			
R_p (%)	13.90	18.10	17.20
R_{wp} (%)	14.40	15.90	14.80
R_{exp} (%)	6.18	11.24	11.26
Hexaferrite ($SrFe_{12}O_{19}$, $P6_3/mmc$)			
$a = b$ (Å)	5.88285(4)	5.87542(5)	5.87624(5)
c (Å)	23.0828(2)	23.0588(3)	23.0468(3)
Phase fraction (%)	99.7(3)	100.0(3)	93.6(3)
R_{Bragg}	8.57	7.68	6.72
Apparent size $hk0$ (nm)	89(1)	62.3(8)	68.5(9)
Apparent size $00l$ (nm)	35(1)	34(1)	38(1)
Modified March coefficient (G1)	0.8110	0.7322	0.8658
Modified March fraction (1-G2)	0.9173	0.2534	0.2328
Hematite (α-Fe_2O_3, R Error!**c:H)**			
$a = b$ (Å)	5.0471(8)	-	5.0317(2)
c (Å)	13.726(4)	-	13.7266(8)
Phase fraction (%)	0.27(5)	-	6.4(1)
R_{Bragg}	23.20	-	7.84
Apparent size, iso (nm)	-	-	48(2)

The size description follows the FullProf platy model with Thomson-Cox-Hastings pseudo-Voight peak shape, which is described in the FullProf manual[1]. From refined parameters Y and S_Z, the Lorentzian factor Y_L can be calculated as $Y_L = Y + S_Z \cos[\alpha]$ where α is the angle

between the q vector and the hkl direction. The diffractograms are recorded in reflection geometry, meaning $\alpha(00l) = 0$ and $\alpha(hk0) = \pi/2$. Note that FullProf uses a factor $360\cdot10^{-6}\cdot\lambda / \pi^2$ to express S_Z. The apparent size can then be calculated using $D_{\mathrm{h}} = \dfrac{1}{Y_{\mathrm{L}}} \cdot \dfrac{360\lambda}{\pi^2}$ with λ being the X-ray wavelength. The results from the refinements can be seen in Table S1. Precision of apparent sizes for 00l have been rounded up from 5 Å (FullProf output) to ½ a unit cell (approx. 1 nm).

SEM images of precursor powders

SEM images used for the extraction of the size distribution can be seen in Figure S1-S3. The samples are the three powders MRT, M600 & M1000, mounted on sticky carbon on a SEM stub. Pressurised air was blown onto the sample on the sticky carbon in order to remove any loose particles.
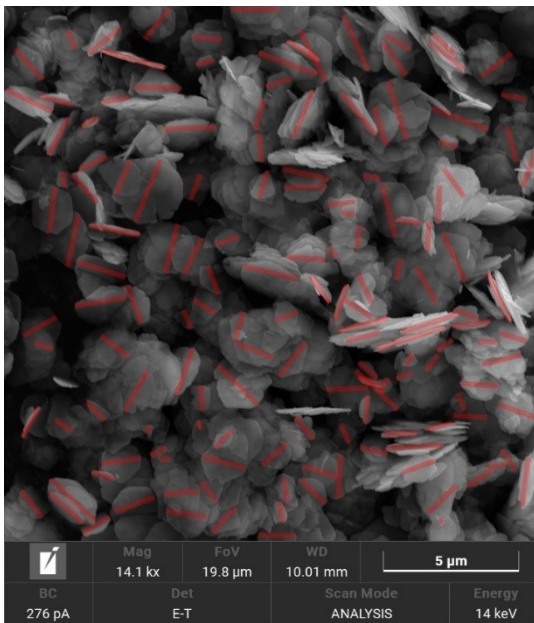

Figure S1: SEM image of powder MRT. Red lines show the measurements used in the size distribution.
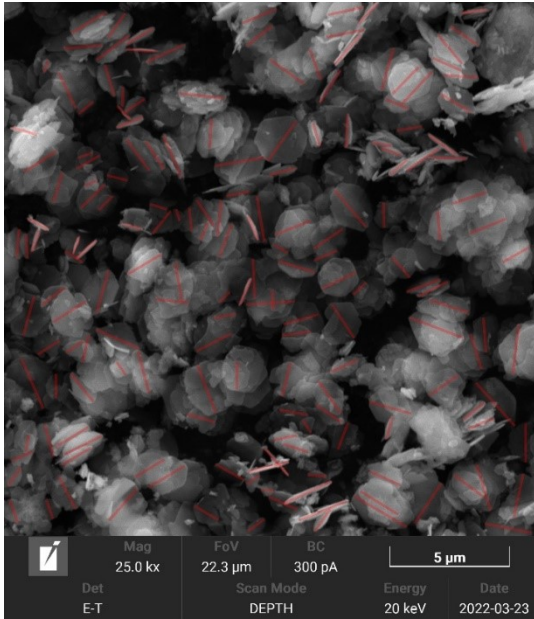
Figure S2: SEM image of powder M600. Red lines show the measurements used in the size distribution.
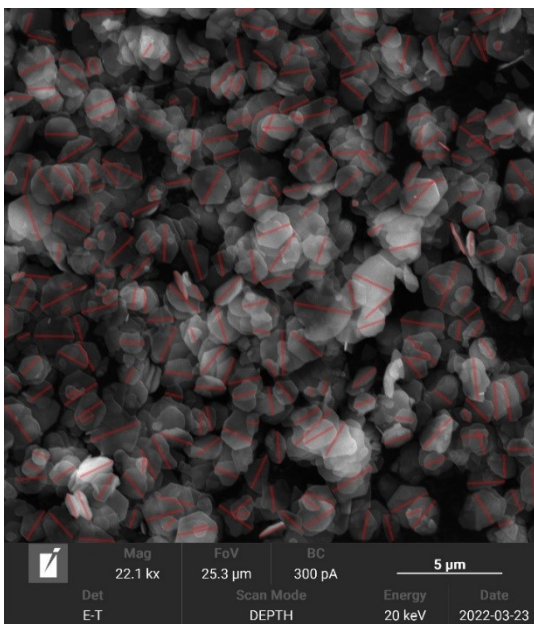

Figure S3: SEM image of powder M1000. Red lines show the measurements used in the size distribution.

The measured sizes from Figure S1, Figure S2 & Figure S3 resulted in size distributions. These were fitted with LogNorm function in OriginPro 2023 10.0.0.154. The result of the measurements can be seen in Table S2, where the fitting function used was:

$$y = y_0 + \frac{A}{\sqrt{2\pi}wx} \exp\left[-\frac{\ln\left(\frac{x}{xc}\right)^2}{2w^2} \right]$$

With refined parameters $0 \leq y_0$, $0 < xc$, $0 < w$ and A. From the refined parameters, mean μ is calculated with $\mu = \exp\left[\ln(xc) + \frac{w^2}{2}\right]$ and shape parameter σ with $\sigma = \mu \cdot \sqrt{\exp\left[w^2\right] - 1}$.

In addition, particles oriented with their platelet normal parallel to the SEM stub surface were located for each sample, allowing for single measurements of particle thicknesses, as seen in Figure S4-S6. These individual measurements are listed for each powder in Table S2.
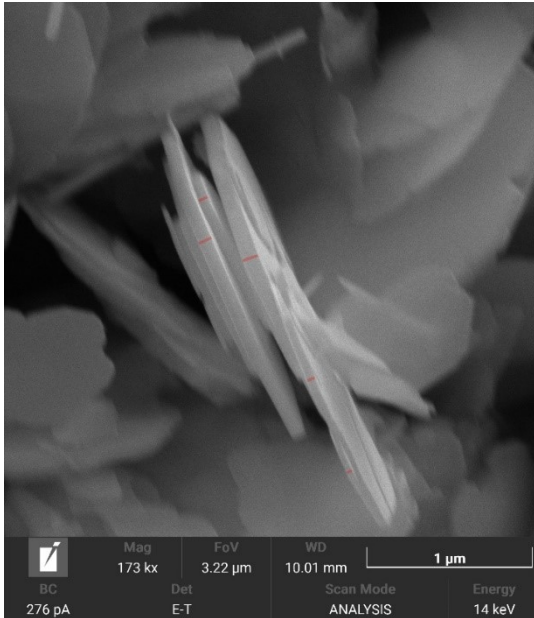

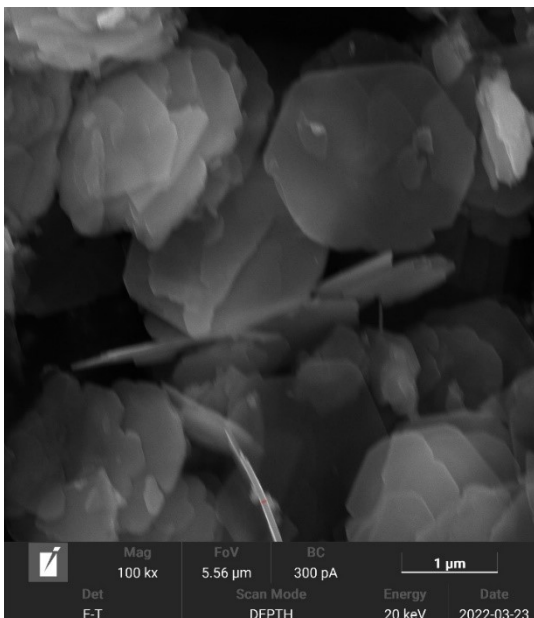*Figure S4: Thickness of particles in powder M. Red lines show measured dimensions (centre of image).*

Figure S5: Thickness of a particle in powder M600. Red line shows measured dimension (bottom-centre of image).
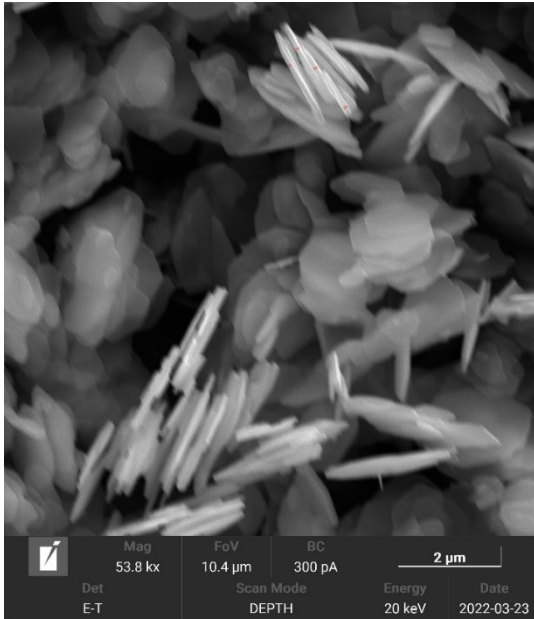
Figure S6: Thickness of particles in powder M1000. Red lines show measured dimensions (top of image).

Table S2: Measured thicknesses of particles and LogNorm parameters along with their standard deviations for powders M, M600 & M1000.

	M	M600	M1000
Individual thickness measurements (nm)	33	59	32
	47		36
	82		41
	56		43
	96		
LogNorm fitting parameters			
y_0 (1/nm)	0 ± 3.34	0 ± 5.41	0 ± 6.21
xc (nm)	263 ± 21	271 ± 17	263 ± 21
w	0.477 ± 0.082	0.363 ± 0.075	0.467 ± 0.084
A	8025 ± 2196	9215 ± 2885	15311 ± 4173
μ (nm)	294 ± 33	290 ± 24	293 ± 32
σ (nm)	149 ± 44	109 ± 32	145 ± 44
Reduced χ^2	15 ± 1	34 ± 1	57 ± 1

Spark plasma sintering profiles and programs

The temperature, pressure, and displacement profiles (lines) along with the planned compaction program (shades) for M-SPS, M600-SPS and M1000-SPS can be seen in Figure S7. Below 600°C, the pyrometer used for measuring the temperature could not gauge the temperature. The main change in displacement is interpreted as the sintering of the powder into a pellet. It is interesting to note that the displacement already happens on the approach to the final temperature, and not during the holding time.
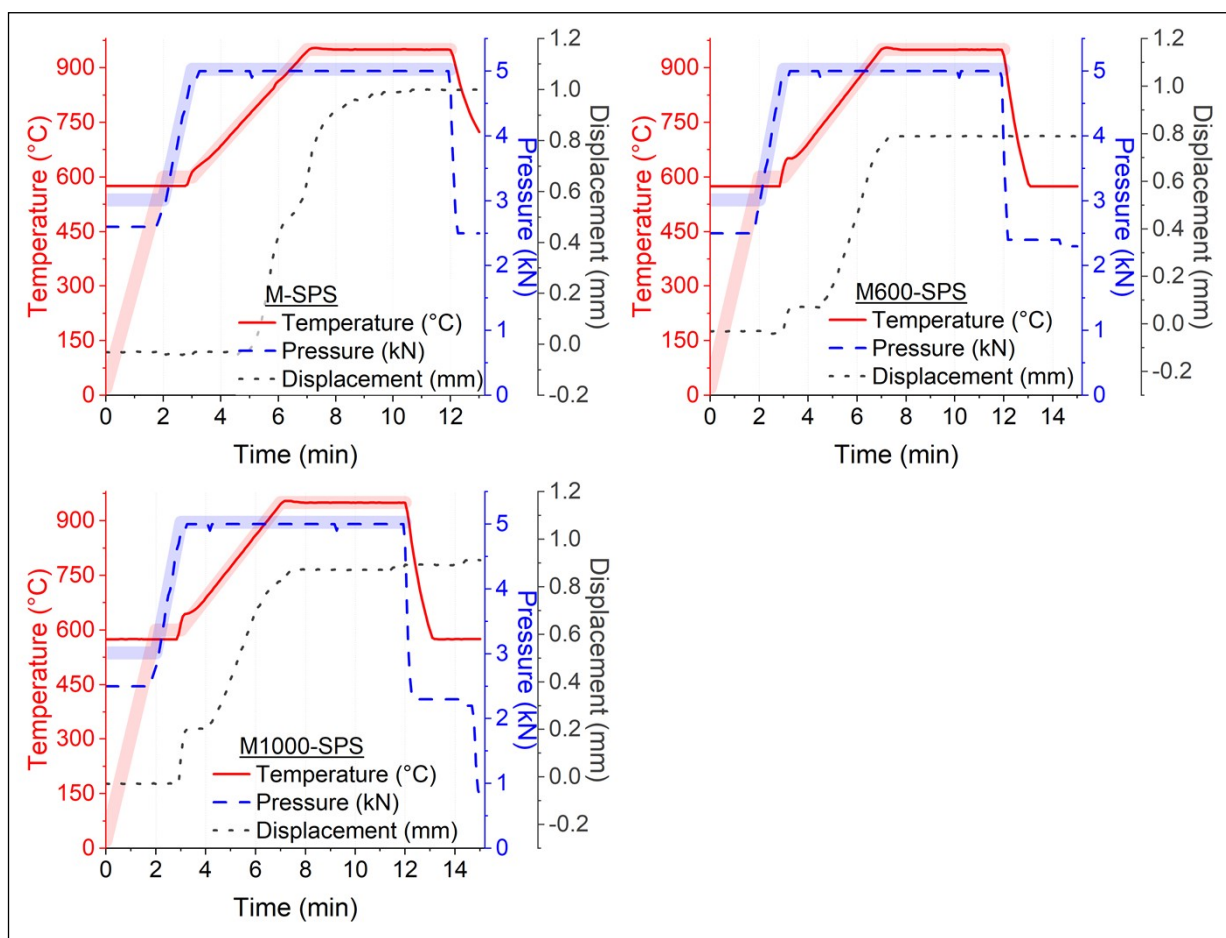
Figure S7: temperature, pressure and displacement profiles for M-SPS, M600-SPS and M1000-SPS. The shadow for temperature and pressure shows the program, and the lines shows the measured value during compaction.

2D diffractograms

Each pellet had four diffractograms recorded with varying φ angle, so that the pellet normal made a φ = 0°, 15°, 30°, 45° angle to the X-ray beam on the detector side, rotated around a horizonal axis perpendicular to the X-ray beam. A sketch of the angle definitions used in this paper can be seen in Figure S8. Each of these 2D diffractograms were caked into 72 1D diffractograms, meaning every 1D diffractogram represents a $\Delta\eta$ = 5° (azimuthally) slice. Vertical line on the bottom half of the detector defines η = 0°. Stacking the 72 diffractograms in η order produces a heatmap of observed intensities (Obs.) as seen in Figure S8-S11 (left columns). For each sample, only the diffractogram with φ = 45° is displayed, as this is the orientation that displays the largest variation along the azimuthal direction η, making clear the texture information present in the diffractograms.
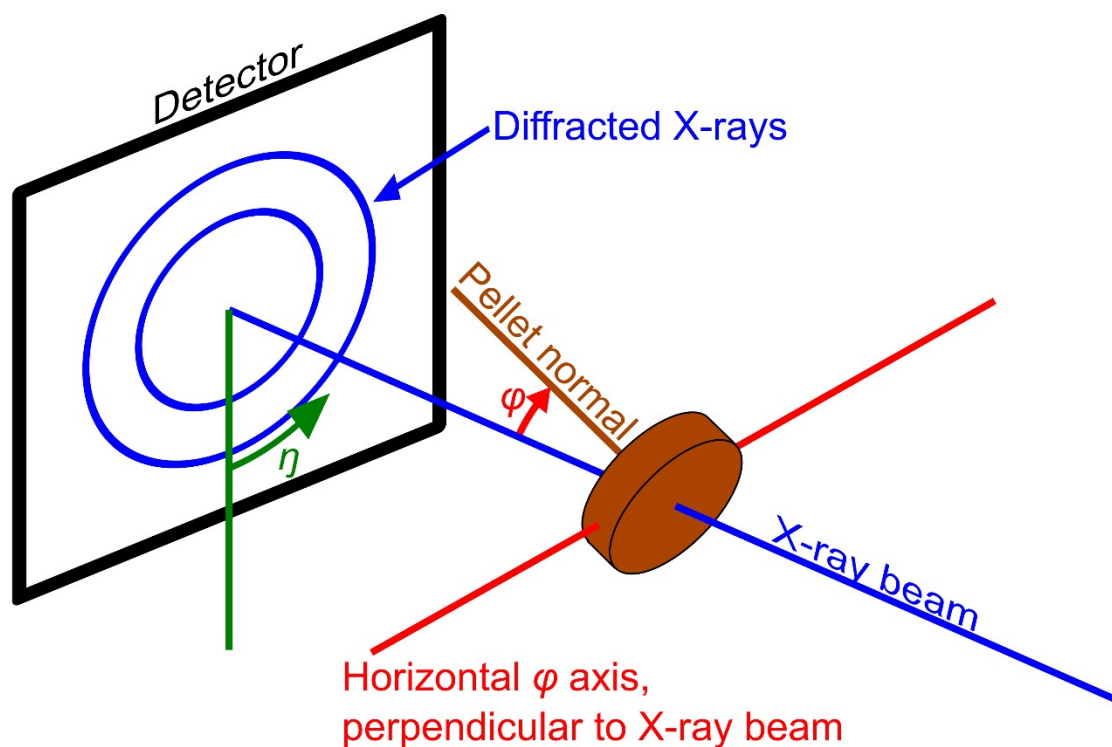
Figure S8: Sketch of angle definitions φ and η used in this paper.

As each sample has four 2D diffractograms recorded, each caked into 72 1D diffractograms, this makes 288 1D diffractograms per sample, with a few blank due to beamstop position near $\eta = 0°$. A Rietveld refinement was performed in MAUD[2] as described in the main article, using all 288 diffractograms in a single, unified refinement. The residuals (Res.) from these models are shown in Figure S8-S11 (right columns). The linear scales are chosen from 0 to 75% of maximal observed intensity for the observed, and residual plots are displayed with −10% to +10% relative to maximum observed intensity. Any values exceeding the limits are coloured with the limits' colour. An artefact around $\eta = 0\text{-}60°$ can be seen in all diffractograms, this is a line of bad pixels.
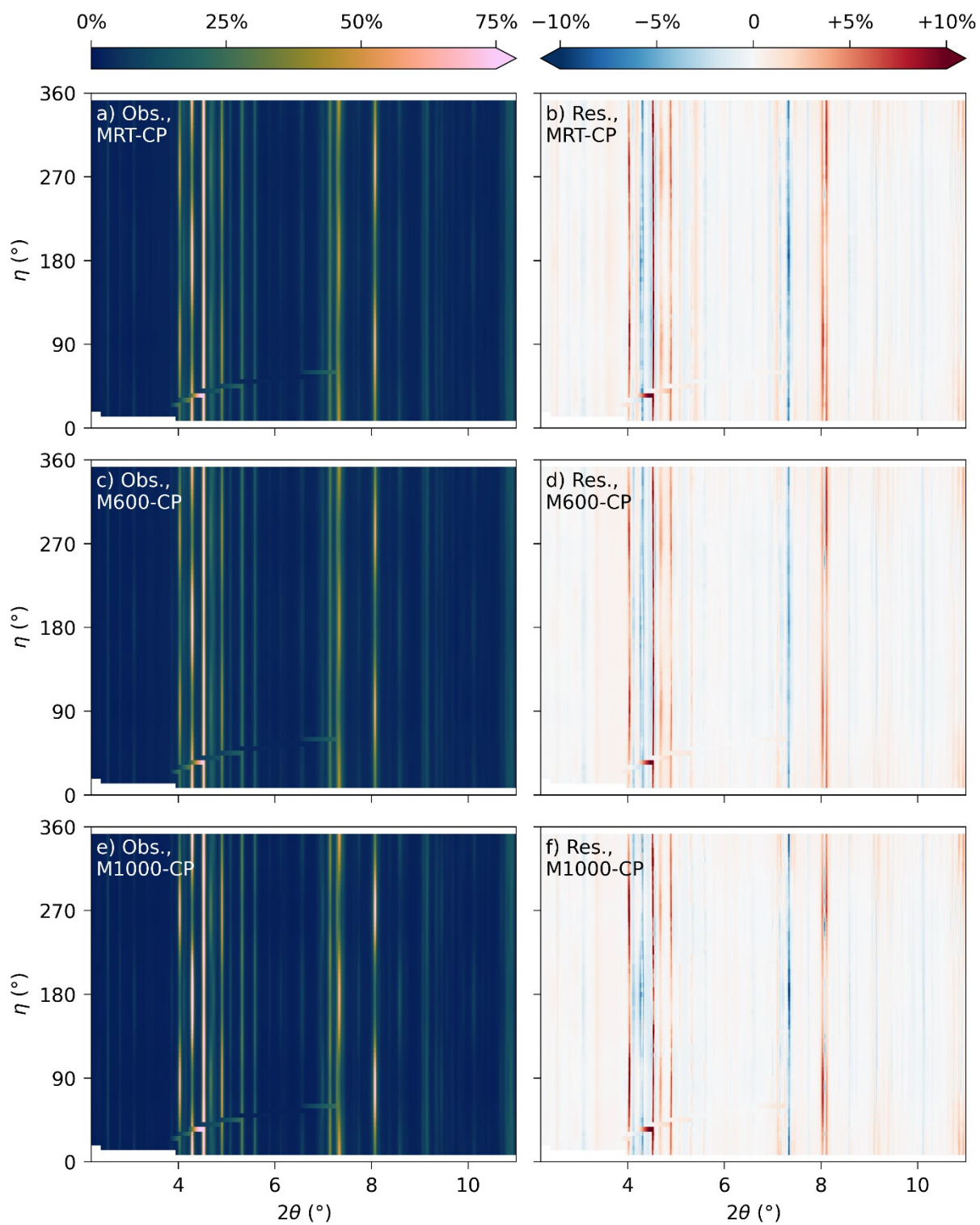
Figure S9: 2D X-ray diffraction patterns for samples M-CP, M600-CP and M1000-CP (linear scale).
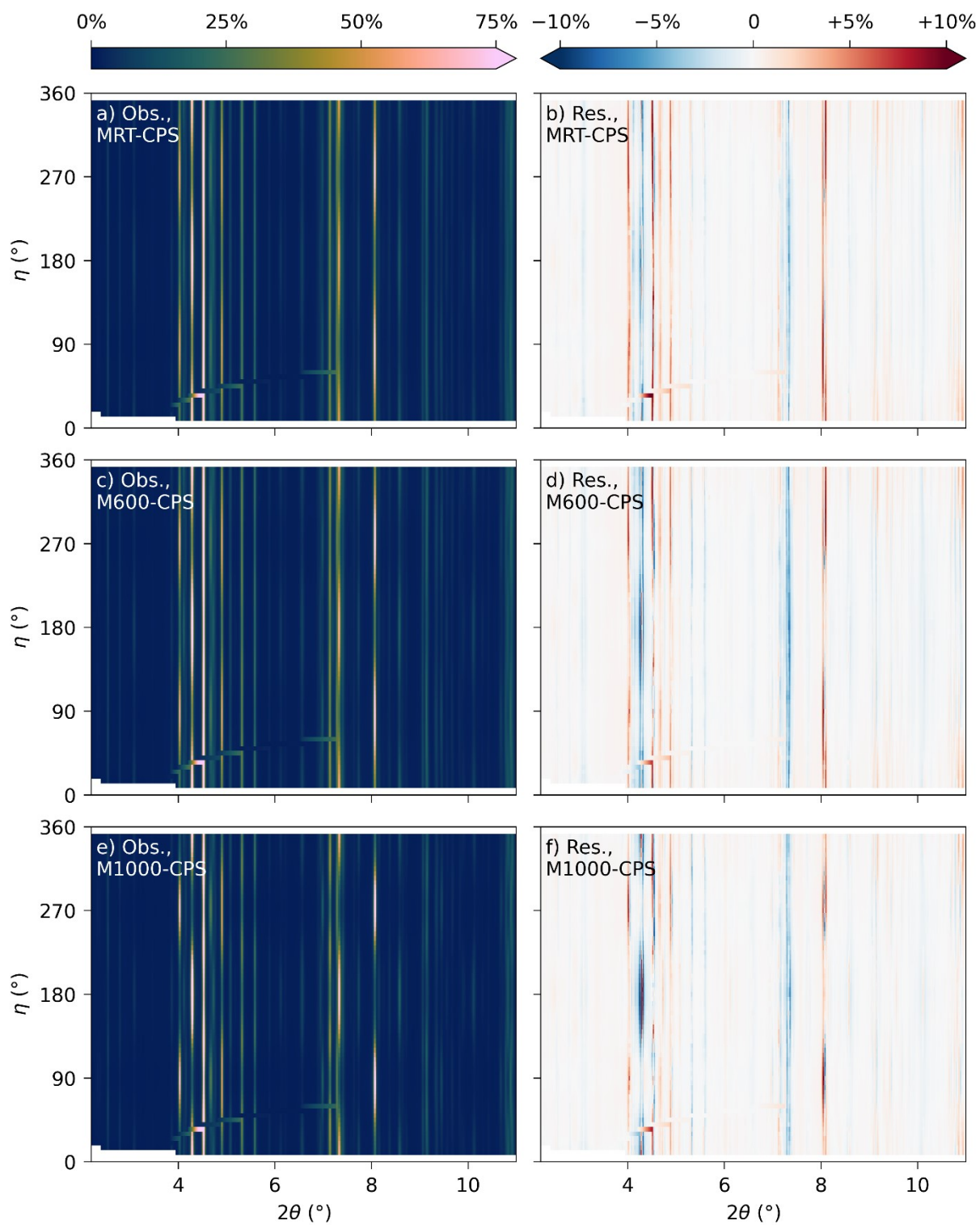
Figure S10: 2D X-ray diffraction patterns for samples M-CSP, M600-CPS and M1000-CPS (linear scale).
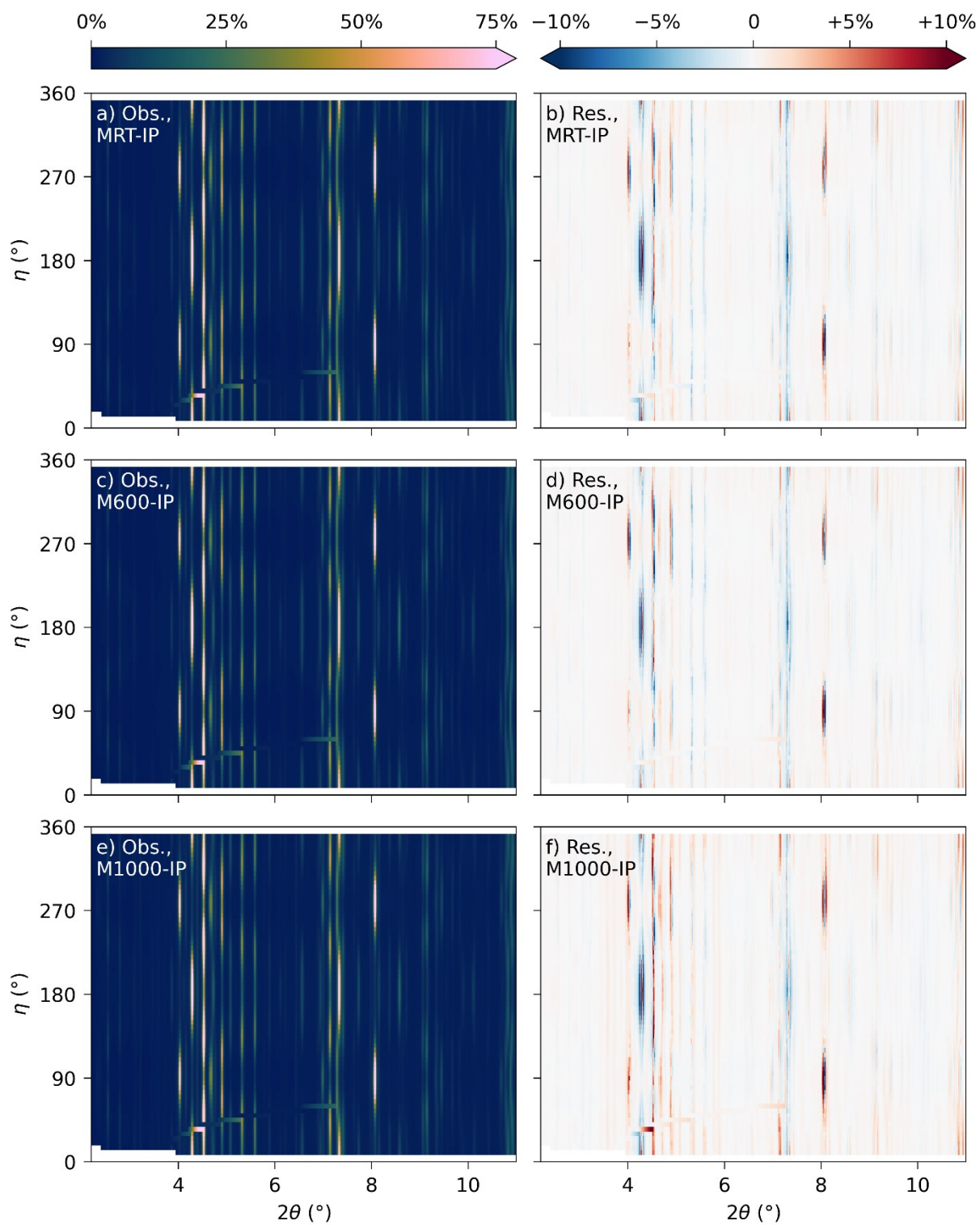
Figure S11: 2D X-ray diffraction patterns for samples M-IP, M600-IP and M1000-IP (linear scale).
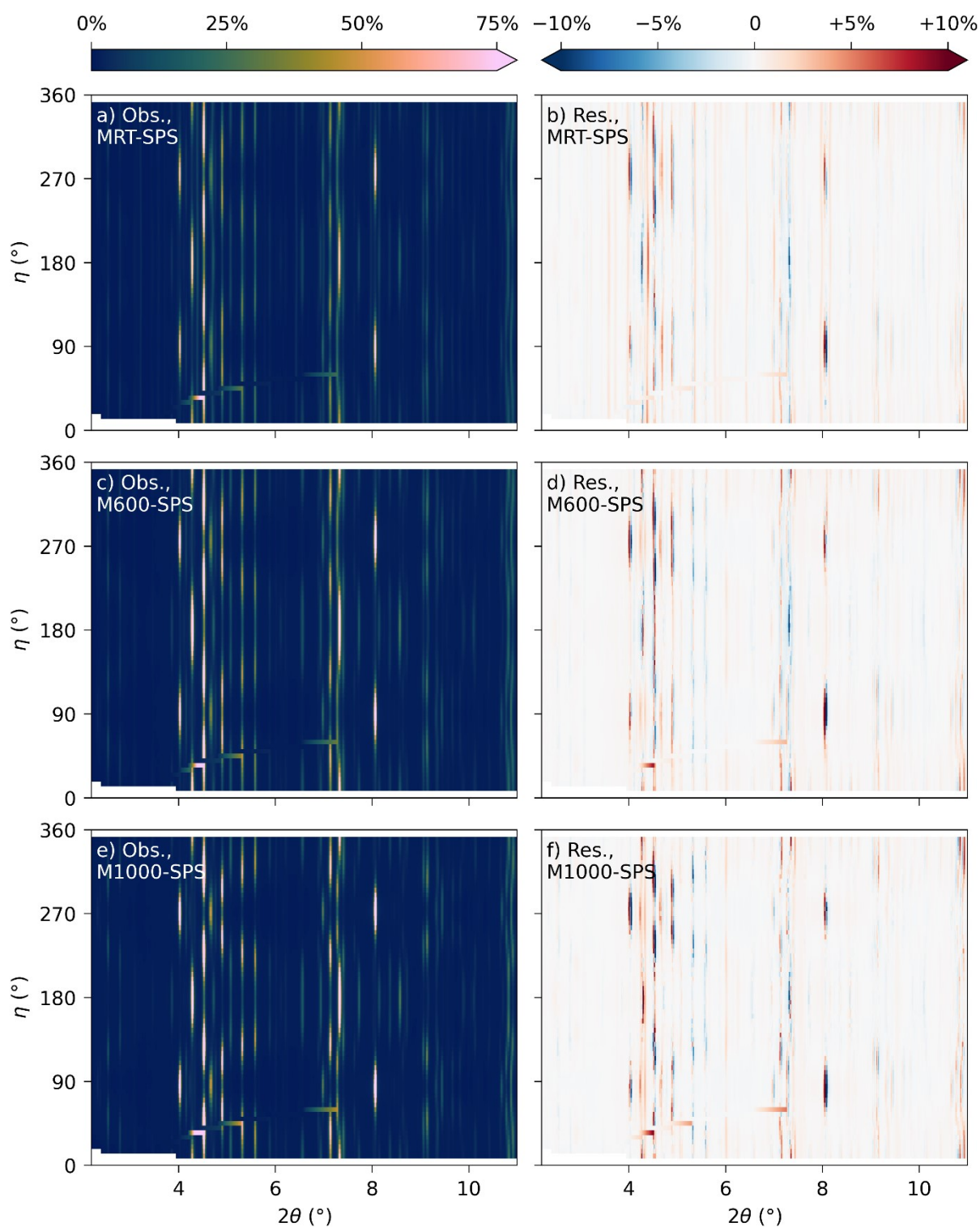
Figure S12: 2D X-ray diffraction patterns for samples M-SPS, M600-SPS and M1000-SPS (linear scale).

Table S3-S6 below summarises the results from the refinements in MAUD. The scale factor for the hexaferrite phase was fixed to 1, and the scale factor for α-Fe_2O_3 (if present) was then refined. The weight fraction of hexaferrite was calculated from the scale factor as *hex wt,% =* $\rho_{hex} \cdot S_{hex}/(\rho_{hex} \cdot S_{hex} + \rho_{hem} \cdot S_{hem})$ with S being the scale factor and ρ being the density, hex short

for hexaferrite and hem short for hematite. In the tables for MAUD parameters, app. is short for apparent and F^2 is the MAUD built-in texture index calculation, note this is equal to the square of the texture strength F.

The determination of crystallite size from peak broadening is in part limited by the resolution of the detector, an estimate of this follows. A single pixel spans $\Delta 2\theta = \arctan(p/d)$ where p is the pixel dimension in mm and d is the distance from the sample to the pixel in mm. Setting this as the integral breath in the Scherrer formula, $L_{centre} = 0.9 \cdot \lambda \,/\, \cos(2\theta/2) \cdot \Delta 2\theta$, with $\lambda = 0.20709$ Å as the wavelength of the incoming radiation. Using a pixel at the centre of the detector with $p = 0.200$ mm, $d = 1001.9$ mm and $2\theta = 0°$ yields a $L_{centre} = 93$ nm. Using a pixel at the corner of the detector with $p = 0.283$ mm, $d = 1027.7$ mm and $2\theta = 5.5°$ yields $L_{corner} = 96$ nm. From these rough estimates, the resolution of the detector limits the reliability of crystallite sizes from peak broadening to maximum ~ 100 nm.

Table S3: shows numerical values extracted from MAUD refinement of the CP series. M1000-CP did not have enough peak intensity to perform profile analysis to estimate crystallite size.

	MRT-CP	M600-CP	M1000-CP
Quality of fit factors			
R_p (%)	8.75	8.24	6.48
R_p, no background (%)	12.3	11.5	8.53
R_{wp} (%)	11.0	10.4	8.38
R_{wp}, no background (%)	14.4	13.7	10.4
M-type Sr hexaferrite ($SrFe_{12}O_{19}$, $P6_3/mmc$)			
a, b (Å)	5.88450(1)	5.88368(1)	5.884669(8)
c (Å)	23.0937(1)	23.0723(1)	23.0592(1)
App. size for a, b (nm)	57.84(3)	59.01(2)	55.09(5)
App. size for c (nm)	40.40(2)	36.69(2)	52.42(2)
MAUD F^2 (m.r.d.^{2})	1.48	1.35	2.30
Hematite (α-Fe_2O_3, RError!c:H)			
Mass fraction (%)	0.68(2)	0.96(2)	0.22(1)
$a = b$ (Å)	5.054(2)	5.054(1)	5.0578(8)
c (Å)	13.479(6)	13.619(5)	13.686(3)
App. size, isotropic (nm)	22.7(6)	19.3(5)	-

Table S4: shows numerical values extracted from MAUD refinement of the CPS series.

	MRT-CPS	M600-CPS	M1000-CPS
Quality of fit factors			
R_p (%)	7.56	7.35	6.06
R_p, no background (%)	9.89	9.63	8.16

R_{wp} (%)	9.95	9.98	8.20
R_{wp}, no background (%)	12.2	12.3	10.2
M-type Sr Hexaferrite ($SrFe_{12}O_{19}$, P6$_3$/mmc)			
a, b (Å)	5.888558(7)	5.887167(8)	5.885494(1)
c (Å)	23.08235(7)	23.07766(9)	23.06838(3)
App. size for a, b (nm)	196.7(1)	288.8(3)	152.5(2)
App. size for c (nm)	67.78(2)	48.83(5)	97.92(4)
MAUD F^2 (m.r.d.^{2})	1.41	1.48	2.82

Table S5: shows numerical values extracted from MAUD refinement of the IP series.

	MRT-IP	M600-IP	M1000-IP
Quality of fit factors			
R_p (%)	8.68	8.41	10.8
R_p, no background (%)	11.2	11.0	12.0
R_{wp} (%)	12.0	11.5	14.9
R_{wp}, no background (%)	14.4	14.0	17.9
M-type Sr Hexaferrite ($SrFe_{12}O_{19}$, P6$_3$/mmc)			
a, b (Å)	5.885875(2)	5.886549(2)	5.884054(9)
c (Å)	23.09437(3)	23.09571(3)	23.0843(2)
App. size for a, b (nm)	386.0(1)	351.5(1)	303.6(1)
App. size for c (nm)	29.80(5)	55.93(5)	34.3(1)
MAUD F^2 (m.r.d.^{2})	5.95	6.70	6.69
Hematite (α-Fe_2O_3, R**Error!**c:H)			
Mass fraction (%)	-	-	7.7(9)
$a = b$ (Å)	-	-	5.0475(2)
c (Å)	-	-	13.7492(7)
App. size, isotropic (nm)	-	-	20.63(4)

Table S6: shows numerical values extracted from MAUD refinement of the SPS series.

	MRT-SPS	M600-SPS	M1000-SPS
Quality of fit factors			
R_p (%)	8.03	7.85	8.29
R_p, no background (%)	9.03	10.2	10.9
R_{wp} (%)	11.1	11.2	12.3
R_{wp}, no background (%)	13.7	13.4	15.0
M-type Sr Hexaferrite ($SrFe_{12}O_{19}$, P6$_3$/mmc)			
a, b (Å)	5.889751(6)	5.888824(6)	5.888100(6)
c (Å)	23.1193(1)	23.1060(1)	23.0958(1)
App. size for a, b (nm)	224.6(6)	304.9(9)	344.1(8)
App. size for c (nm)	150.3(4)	110.2(3)	188.4(6)
MAUD F^2 (m.r.d.^{2})	7.50	8.17	13.96
Hematite (α-Fe_2O_3, R**Error!**c:H)			
Mass fraction (%)	8.7(1)	-	-

$a = b$ (Å)	5.04886(4)	-	-
c (Å)	13.7714(2)	-	-
App. size, isotropic (nm)	191(2)	-	-

Energy product as function of coercivity

Figure S12 shows the energy product as a function of coercivity. The trend is weak and negative, indicating that the energy product is not limited by coercivity for the pellets in this paper. The exception might be the two samples with the lowest coercivities M1000-IP and M1000-SPS. For the coercivity to be the limiting factor, $H_C < M_R/2$ can be used as a rough estimate, with M_S expressed as a volume magnetisation. Using some representative values from table 2, $M_R = 0.9 \cdot 73$ A m^2 kg^{-1}, $\rho = 4.8$ g cm^{-3}, the coercivity limit is $M_R/2 = 158$ kA m^{-1}. According to this estimate, the energy product of M1000-IP and M1000-SPS are limited by coercivity.
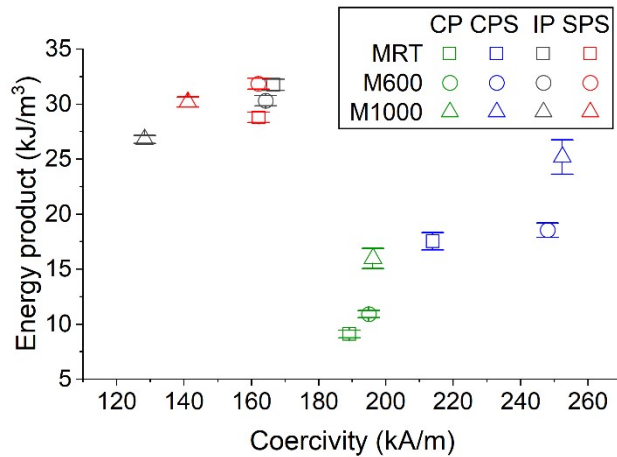

Figure S13: Energy product as function of coercivity. No clear positive trend is apparent, indicating that coercivity is generally not the limiting factor for energy product in this study.

Magnetisation curves perpendicular to pressing direction

Hysteresis loops of magnetisation were measured for the six hot compacted pellets as seen in Figure S14b,c. Demagnetisation correction to infinite slope was not performed for these. A demonstration of the anisotropy of the pellets can be seen by the example of M600-IP, which have the hysteresis loop recorded with four different angles between the applied H and the pressing direction, Figure S14a. In Figure S14a, the same demagnetisation correction method (infinite slope) has been performed for all loops for comparison, but note that this becomes less suitable the larger the angle.
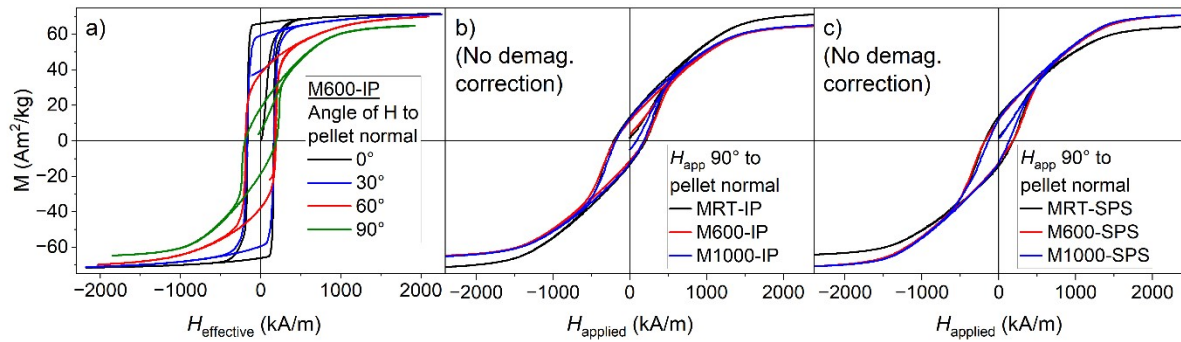
Figure S14: shows hysteresis curves measured with the VSM, a) M600-IP sample measured with the applied H at four different angles to the pressing axis, b) all IP pellets measured with H applied perpendicular to the pressing axis and c) all SPS pellets measured with H applied perpendicular to the pressing axis.

Bibliography for supplementary

1. Rodríguez-Carvajal J. Introduction to the program FullProf: Refinement of crystal and magnetic structures from powder and single crystal data. Lab Léon Brillouin. 2001;

2. Lutterotti L, Bortolotti M, Ischia G, Lonardelli I, Wenk HR. Rietveld texture analysis from diffraction images. Z Kristallogr Suppl. 2007 Nov;2007(26):125–30.